

# Simulating complex quantum networks with time crystals

M. P. Estarellas,<sup>1,\*</sup> T. Osada,<sup>2,1,\*</sup> V. M. Bastidas,<sup>3,\*</sup> B. Renoust,<sup>4,1,5</sup> K. Sanaka,<sup>2</sup> W. J. Munro,<sup>3,1</sup> and K. Nemoto<sup>1,5</sup>

<sup>1</sup>*National Institute of Informatics, 2-1-2 Hitotsubashi, Chiyoda-ku, Tokyo 101-8430, Japan*

<sup>2</sup>*Tokyo University of Science, 1-3 Kagurazaka, Shinjuku, Tokyo, 162-8601, Japan*

<sup>3</sup>*NTT Basic Research Laboratories & Research Center for Theoretical Quantum Physics, 3-1 Morinosato-Wakamiya, Atsugi, Kanagawa, 243-0198, Japan*

<sup>4</sup>*Osaka University, Institute for Datability Science, 2-8 Yamadaoka, Suita, Osaka Prefecture 565-0871, Japan*

<sup>5</sup>*Japanese-French Laboratory for Informatics, CNRS UMI 3527, 2-1-2 Hitotsubashi, Chiyoda-ku, Tokyo 101-8430, Japan*

(Dated: April 7, 2022)

Crystals arise as a result of the breaking of a spatial translation symmetry. Similarly, periodically-driven systems host non-equilibrium states when discrete symmetries in time are broken. These exotic phases are often referred to as time crystals. Here we introduce a novel method to describe, characterize and explore the physical phenomena related to this new phase of matter using tools from graph theory. This not only allows us to visualize time-crystalline order, but also to analyze features of the quantum system through the analysis of graphs. As an example, we explore in detail the melting process of a 2T Discrete Time Crystal (2T-DTC) and describe it in terms of the evolution of the associated graph structure. We show that during the melting process, the evolution of the network exhibits an emergent preferential attachment mechanism, directly associated to the existence of scale-free networks. Thus our strategy allows us to propose a new far-reaching application of time crystals as a quantum simulator of complex quantum networks.

## I. INTRODUCTION

Symmetries are of utmost importance in condensed matter physics and statistical mechanics due to the strong relation between quantum phases of matter and symmetry breaking [1–4]. Among the zoo of symmetry broken phases, discrete time crystals (DTC) play a fundamental role on their own due to the type of symmetry involved [5]. The time-crystalline phase, analogous to “space” crystals, arises when time (instead of space) translation symmetry is broken. The existence of quantum time crystals was originally proposed by Wilczek [6], and discrete version of time crystals can be realized periodically-driven quantum systems [7–9]. It is in such cases that the system dynamics exhibits a subharmonic response with respect to the characteristic period of the drive caused by the synchronization in time of the particles of a many-body system [5].

The exploration of time crystals is a very active field of research and several experimental realizations with trapped ions [10], dipolar spin impurities in diamond [11], and ordered dipolar many-body systems [12] have been achieved. Yet an intuitive and complete insight of the nature of time-crystals and its characterization, as well as a set of proposed applications, is lacking. We here provide new tools based on graph theory and statistical mechanics to fill this gap. We propose a new strategy for the study and understanding of time symmetry-broken phases and their related phenomena [13, 14]. As an example, we characterize the time-crystalline order and its melting.

Our approach allows us to identify perturbed time-crystals as a novel physical platform where to simulate complex networks whose evolution is governed by preferential attachment mechanisms [15, 16]. This type of networks, far from being regular or random, contains non-trivial topological structures present in many biological, social and technological systems. Small-world and scale-free networks are two of the

most popular examples, the later being commonly characterized through power-law degree distributions that can be explained from the presence of a preferential attachment mechanism. The simulation of such networks has wide applicability, ranging from the study and understanding of behaviors present in communication or internet networks [17], the development of new algorithms in deep learning [18], or the analysis of genetic and neural structures in biological systems [19].

## II. FLOQUET THEORY IN A NUTSHELL

The fundamentals of this work rely on the exploration of the dynamics of driven many-body quantum systems described by time-periodic Hamiltonians  $\hat{H}(t+T) = \hat{H}(t)$ , with  $T = 2\pi/\omega$  being the period of that drive. Our approach builds from the calculation of the Floquet operator  $\hat{\mathcal{F}} = \hat{U}(T) = \mathcal{T} \exp(-i \int_0^T \hat{H}(\tau) d\tau / \hbar)$ , which is the evolution operator within one period from time  $t = 0$  to time  $t = T$  [20–22] with  $\mathcal{T}$  being the time ordering operator. In Floquet theory, one wishes to solve the eigenvalue problem  $\hat{\mathcal{F}}|\Phi_s\rangle = e^{-i\lambda_s T/\hbar}|\Phi_s\rangle$ . The eigenvectors  $|\Phi_s\rangle$  are known as Floquet states and  $-\hbar\omega/2 \leq \lambda_s \leq \hbar\omega/2$  are the quasienergies. At discrete times  $t_n = nT$ , the evolution can be understood in terms of an effective “time-independent” Hamiltonian  $\hat{H}^{\text{eff}}$  such that  $\hat{\mathcal{F}} = e^{-i\hat{H}^{\text{eff}} T/\hbar}$ . This Hamiltonian is very relevant in the context of Floquet engineering as it contains effective interactions that are absent in equilibrium systems, allowing it to be applied to quantum simulation problems [21, 23, 24].

## III. DISCRETE TIME CRYSTALS OF PERIOD 2T

We now move to a well-known Period-2 Discrete Time Crystal (2T-DTC) [10, 13] consisting of a one dimensional chain with  $n$  spin-1/2 particles and governed by a time-

\* These authors contributed equally.

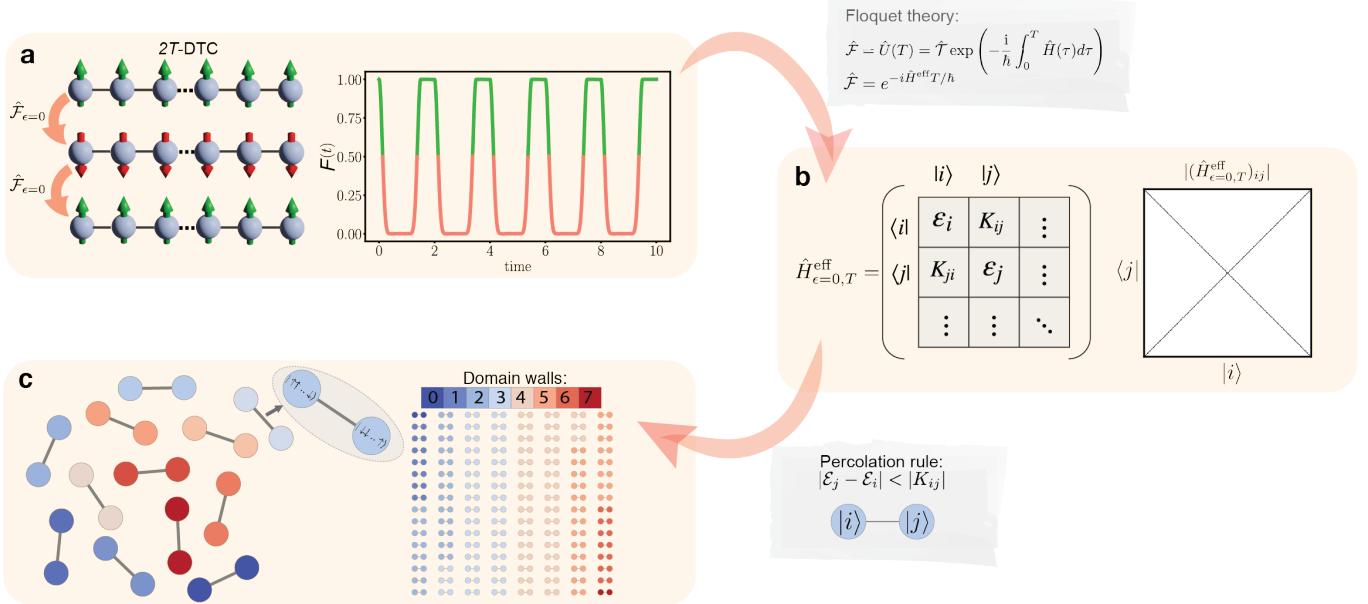


**Figure 1. Obtaining the associated graph of a 2T-DTC.** **a**, On the left, diagram of the 2T-DTC dynamics with no rotation error,  $\epsilon$ . The initial state ( $|\Psi(0)\rangle = |\uparrow\uparrow\uparrow\cdots\uparrow\rangle$ ), represented with the green arrows pointing up, is recovered after two periods of the driving protocol. From the first period, we obtain the unitary,  $U(T)$ , that will be used as the Floquet operator,  $\hat{\mathcal{F}}_{\epsilon=0}$ , to derive the effective Hamiltonian,  $\hat{H}_{\epsilon=0,T}^{\text{eff}}$ . On the right, fidelity of evolving state of an  $n = 8$  sites 2T-DTC against its initial state,  $F(t) = |\langle\Psi(0)|\Psi(t)\rangle|^2$  showing the 2T periodicity of the dynamics. **b**, The effective Hamiltonian,  $\hat{H}_{\epsilon=0,T}^{\text{eff}}$ , represented as a tight-binding matrix.  $\mathcal{E}_i$  and  $K_{ij}$  are the energies of the  $|i\rangle$  configuration (see main text for full description) and transition energy between configurations  $|i\rangle$  and  $|j\rangle$ , respectively. The right panel shows the entries of the effective Hamiltonian matrix, where only the diagonal and anti-diagonal entries are non-zero. **c**, After applying the percolation rule to the effective Hamiltonian we obtain an adjacency matrix, which is in turn represented as a graph with the nodes being each of the  $2^n$  configuration basis set of the Hilbert space. In the right, for no rotation error, the crystal order of the 2T-DTC can be observed as  $2^{n-1}$  decoupled dimers. This crystalline order is present for crystals of other periodicity (as triangles for a 3T-DTC, squares for a 4T-DTC, etc.). Here, the elements of each dimer are the configurations  $|i\rangle$  and  $|2^n - 1 - i\rangle$ , which are related by a global  $\pi$  rotation along the  $x$ -axis. All the nodes with same color have the same number of domain walls with the colormap gradient going from dark blue (0 domain walls) to dark red ( $n - 1$  domain walls).

dependent Hamiltonian with period  $T = T_1 + T_2$ ,

$$\hat{H}(t) = \begin{cases} \hat{H}_1 \equiv \hbar g (1 - \epsilon) \sum_l \sigma_l^x & 0 < t < T_1 \\ \hat{H}_2 \equiv \hbar \sum_{lm} J_{lm}^z \sigma_l^z \sigma_m^z + \hbar \sum_l B_l^z \sigma_l^z & T_1 < t < T_2 \end{cases} \quad (1)$$

Here  $\{\sigma_l^x, \sigma_l^y, \sigma_l^z\}$  are the usual Pauli operators on the  $l$ -th spin,  $J_{lm}^z \equiv J_0/|l - m|^\alpha$  is the long-range interaction between spins  $l, m$ , and  $B_l^z \in [0, W]$  is a random longitudinal field. The parameter  $g$  satisfies the condition  $2gT_1 = \pi$  such that  $\hat{U}_1 = \exp(-i\hat{H}_1 T_1/\hbar)$  becomes a global  $\pi$  pulse around the  $x$ -axis, with a rotation error  $\epsilon$  also introduced. The Floquet operator is then given by:

$$\hat{\mathcal{F}}_\epsilon = \hat{U}_\epsilon(T) = \exp\left(-\frac{i}{\hbar}\hat{H}_2 T_2\right) \exp\left(-\frac{i}{\hbar}\hat{H}_1 T_1\right). \quad (2)$$

Crucially, the Floquet operator depends on the error  $\epsilon$ , which determines how the time crystal will melt. In our work, we choose  $\alpha = 1.51$ ,  $J_0 T_2 = 0.06$  with a disorder strength  $WT_2 = \pi$ , which are similar values used in the recent experiment [10]. The key feature of this unitary evolution is that at each period  $T$ , as shown in Fig. 1.a, the system evolves between the states  $|\uparrow\uparrow\cdots\uparrow\rangle$  and  $|\downarrow\downarrow\cdots\downarrow\rangle$ , when the state is initialized at one of

these two. This periodic evolution is robust against moderate errors  $\epsilon$  in  $\hat{H}_1$ .

#### IV. FLOQUET GRAPHS

Let us now introduce the concept of a Floquet graph as the graphical representation of the effective Hamiltonian,  $\hat{H}_{\epsilon,T}^{\text{eff}}$  [25], obtained as  $\hat{H}_{\epsilon,T}^{\text{eff}} = i\hbar/T \log[\hat{\mathcal{F}}_\epsilon]$ . By shifting to the graph theory framework, we can provide a visual and intuitive understanding of the system and use its well-established tools to understand physical phenomena. We discuss the application of percolation to unveil the complex dynamics of time-crystals, even though such ideas can be widely applicable to any periodically-driven (Floquet) system.

The effective Hamiltonian,  $\hat{H}_{\epsilon,T}^{\text{eff}}$ , is defined on a finite and discrete Hilbert space (dimension  $N_{\mathcal{H}}$ ), and can be written as a tight-binding model using the configuration basis states  $\{|i\rangle\}$ , as

$$\hat{H}_{\epsilon,T}^{\text{eff}} = \sum_i \mathcal{E}_i |i\rangle\langle i| + \sum_{i,j} K_{ij} |i\rangle\langle j| = \sum_s \lambda_s |\Phi_s\rangle\langle\Phi_s|, \quad (3)$$

where  $\mathcal{E}_i$  is the energy of configuration  $|i\rangle$ , and  $K_{ij}$  is the tran-

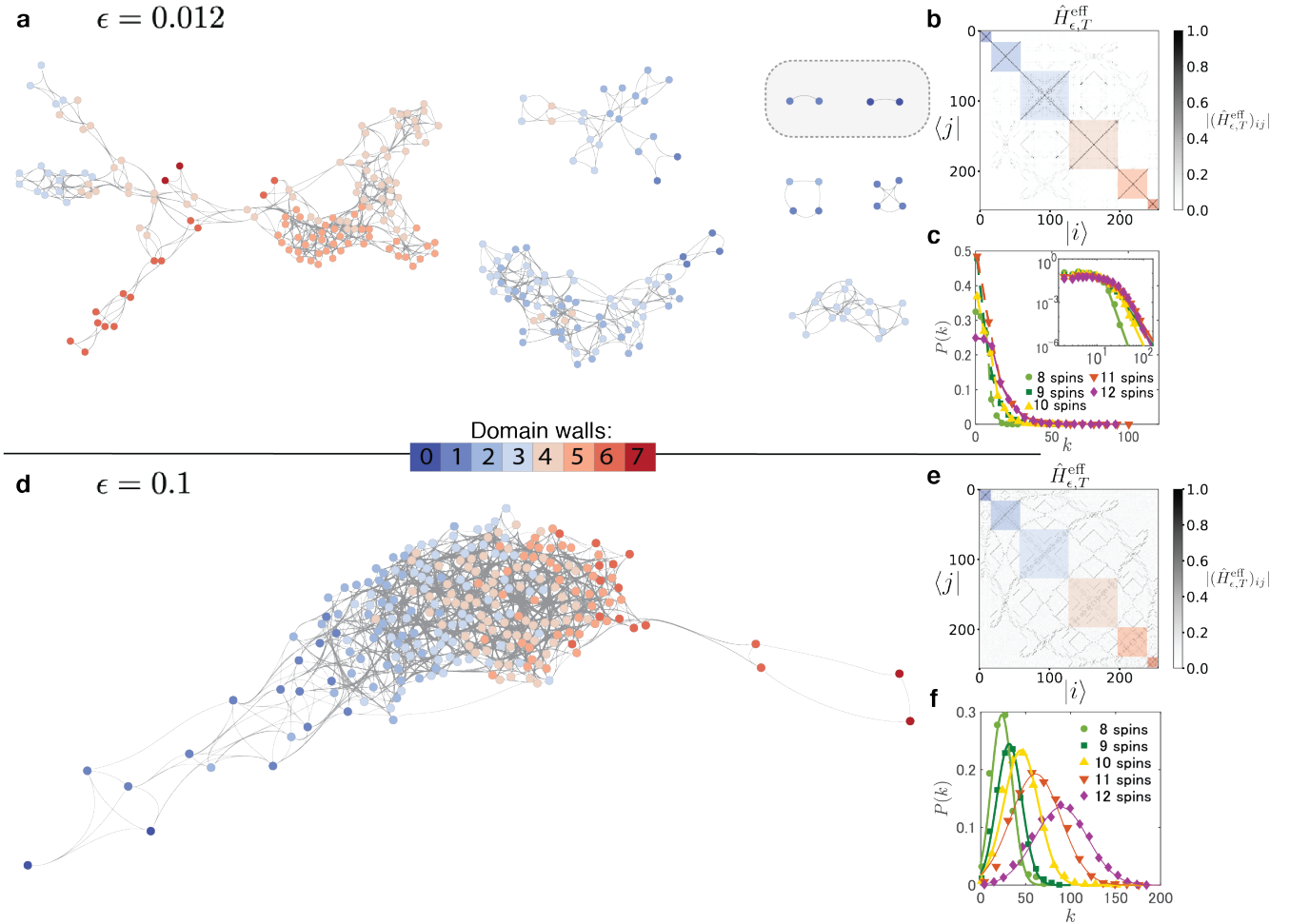


**Figure 2. Melting of a 2T-DTC using  $\hat{H}_{\epsilon,T}^{\text{eff}}$ .** **a**, Graph representation obtained from  $\hat{H}_{\epsilon,T}^{\text{eff}}$  with  $n = 8$  sites and a rotation error of  $\epsilon = 0.012$  with the nodes corresponding to configurations basis set of the Hilbert space color coded according to the number of domain walls of the corresponding state (see colormap). For moderate levels of error the nodes attach to each other according to their number of domain walls: nodes with same or similar number of domain walls are closer in energy; the error lifts the degeneracies present in the spectrum and new transitions between close states appear. This can also be observed in the effective Hamiltonian matrix of panel **b** with the basis ordered in increasing number of domain walls and delimited by the coloured squares. As the nodes start to cluster due to the presence of error, some non-zero off-diagonal terms appear in the centre of the matrix, both inside the same region of 3 domain walls and between 3 and 4 domain walls regions. For this level of error, some dimers survive (see top-right corner of panel **a**), serving as good indication of the robustness of the system and meaning that the crystal order is still present. In panel **c**, the degree distributions of the corresponding graph of panel **a** with different system sizes ( $n = 8 - 12$ ) averaged over 100 realizations of disorder are shown in both linear and logarithmic scale (see inset), which display heavy-tailed distributions. The distributions are fitted with a power-law curve (solid-lines in the inset), indicating the presence of large degree hub nodes. **d**, Graph representation obtained from  $\hat{H}_{\epsilon,T}^{\text{eff}}$  with  $n = 8$  sites and a rotation error of  $\epsilon = 0.1$  with the nodes color coded according to the number of domain walls of the corresponding state (see colormap). **e**, Effective Hamiltonian matrix of a 2T-DTC with  $n = 8$  sites and a rotation error of  $\epsilon = 0.1$ . As we increase the error, the system collapses into a single cluster with high connectivity. This can be seen from the appearance of many new off-diagonal entries in the Hamiltonian matrix as well as the presence of a giant component in the graph. In this scenario, the time crystal has melted completely and no crystal order is left (no presence of isolated dimers). The degree distributions, shown in **f**, also indicates that the heavy-tailed nature is destroyed, and the degree distributions are well approximated to a normal distribution.

sition energy between configurations  $|i\rangle$  and  $|j\rangle$  (see Fig. 1**b**). The Floquet states  $|\Phi_s\rangle$  are linear combinations of the configurations  $|i\rangle$ . In general, the quasienergies  $\lambda_s$  are complicated functions of the parameters  $\mathcal{E}_i$  and  $K_{ij}$ . In this work, we consider a system with  $n$  spin-1/2 particles and the configurations  $\{|i\rangle\}$  with  $i = 0, 1, \dots, 2^n - 1$  can be chosen as the  $N_H = 2^n$  elements of the computational basis, i.e. the product states of the eigenstates of  $\sigma_i^z$ . In general, any configura-

tion can be written as  $|i\rangle = (\sigma_1^+)^{j_1} \dots (\sigma_n^+)^{j_n} |\downarrow\downarrow\dots\downarrow\rangle$ , where  $i = (j_1 j_2 \dots j_n)_2$  is the binary decomposition of the integer  $i$  and  $\sigma_l^+ |\downarrow\rangle_l = |\uparrow\rangle_l$ . By using this notation, the states are denoted as  $|0\rangle = |\downarrow\downarrow\dots\downarrow\rangle$  and  $|2^{n-1}\rangle = |\uparrow\uparrow\dots\uparrow\rangle$ . The configurations satisfy the relation  $|2^n - 1 - i\rangle = \sigma_1^x \sigma_2^x \dots \sigma_n^x |i\rangle$  and will constitute the  $2^n$  nodes of the graph. In addition, such nodes will be linked according to a percolation rule [26], where a non-weighted edge is considered to be active between

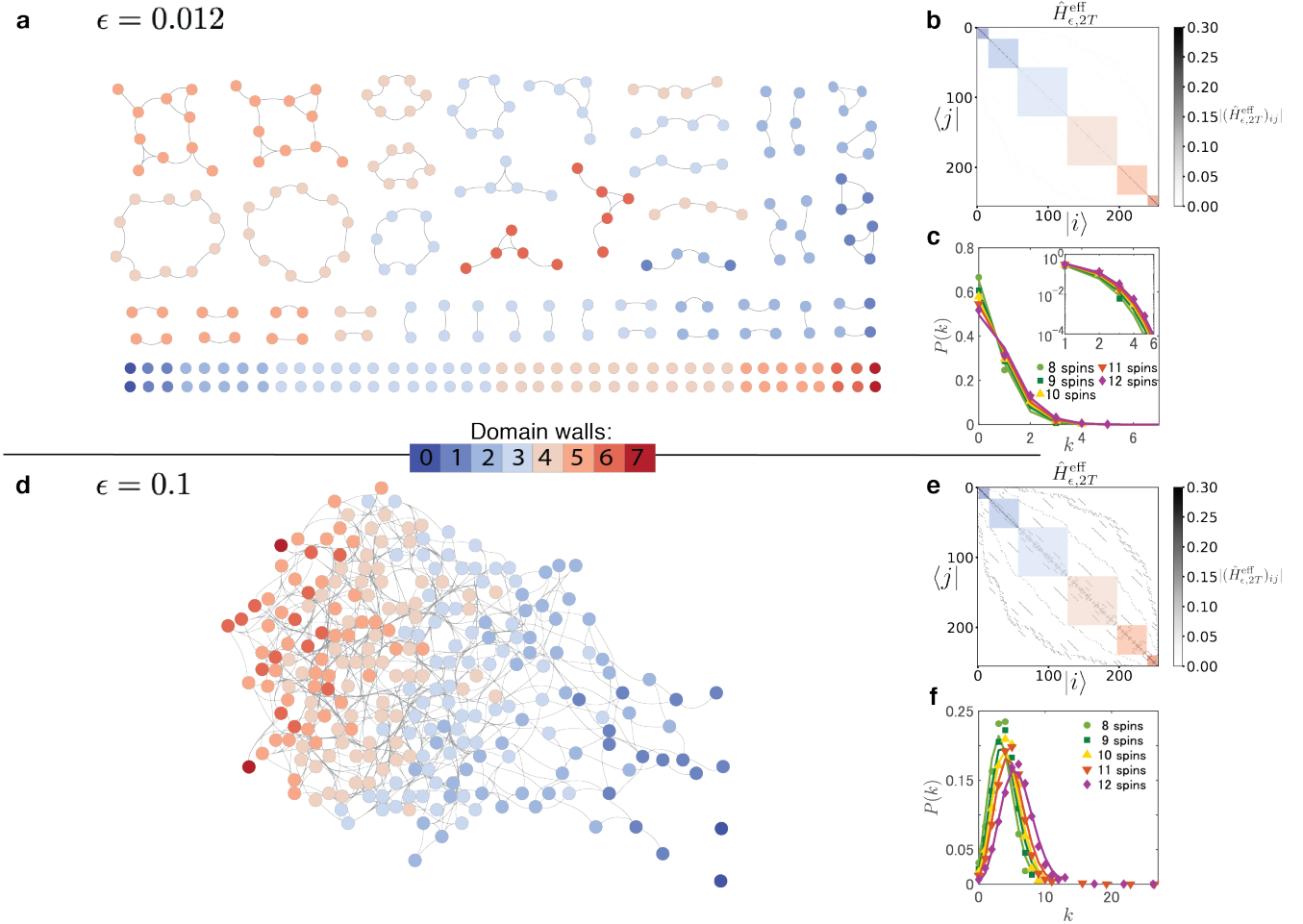


**Figure 3. Melting of a 2T-DTC using  $\hat{H}_{\epsilon,2T}^{\text{eff}}$ .** **a**, Graph representation obtained from  $\hat{H}_{\epsilon,2T}^{\text{eff}}$  with  $n = 8$  sites and a rotation error of  $\epsilon = 0.012$  with the nodes corresponding to configurations basis set of the Hilbert space color coded according to the number of domain walls of the corresponding state (see colormap). For none or moderate levels of error, the nodes are decoupled or forming clusters of small size. In **b**, we present the effective Hamiltonian  $\hat{H}_{\epsilon,2T}^{\text{eff}}$  that presents mainly diagonal terms. For moderate levels of error the nodes form small clusters. Again, they attach to each other according to their number of domain walls. In panel **c**, the degree distributions of the corresponding graph of panel **a** with different system sizes ( $n = 8 - 12$ ) averaged over 100 realizations of disorder are shown in both linear and logarithmic scale (see inset), fitted with a Poisson distribution. This indicates that the corresponding graph is a random graph with low connectivity. **d**, Graph representation obtained from  $\hat{H}_{\epsilon,2T}^{\text{eff}}$  with  $n = 8$  and a rotation error of  $\epsilon = 0.1$ . As we increase the error, the system forms a larger, highly-connected cluster. **e**, This can be seen from the increasing magnitude of the off-diagonal entries in the effective Hamiltonian matrix as well as the presence of a giant component in the graph. In this scenario, the time crystal has melted completely. **f**, The degree distributions are well approximated to a Poisson distribution in the lower degree region, which is the characteristic of highly connected random networks.

nodes  $i$  and  $j$  only if the condition

$$|\mathcal{E}_j - \mathcal{E}_i| < |K_{ij}| \quad (4)$$

is satisfied. This rule eliminates the off-resonant transitions, allowing to effectively visualize the significant transitions in the Hamiltonian.

In order to clarify the percolation on the graph, we define clusters as subsets of nodes which are connected with a path. The graph is percolated when all nodes belong to a single cluster [27]. We want to stress that the nodes represent many-body states  $|i\rangle$  and not physical spin sites  $l$ , so the graph spans through the full Hilbert –configuration– space (see Fig. 1.c).

This percolation rule was proven to be useful to detect many-body localization to thermal phase transitions in undriven spin systems [26].

## V. TIME CRYSTAL GRAPHS

Under the framework of Floquet graphs, the dynamics of the described 2T-DTC can now be investigated. The effective Hamiltonian  $\hat{H}_{\epsilon,T}^{\text{eff}}$  derived from Eq. (2) can be represented as a graph using the percolation rule from Eq. (4). The structure of the graph when  $\epsilon = 0$  presents decoupled dimers (two connected nodes), a signature of 2T-DTCs crystals, as shown in the example presented in Fig. 1.c. We note that this vi-

sual characterization of the crystal time order is not unique of  $2T$ -DTC and can be extrapolated to crystals of different periodicity. For example,  $3T$ -DTC presents decoupled trimers;  $4T$ -DTC presents decoupled tetragons, and so on. Our results hence reveal that, in the case of  $2T$ -DTCs and in the absence of error, there are decoupled two-dimensional subspaces. For example if there is an active link between the configurations  $|0\rangle$  and  $|2^n - 1\rangle$  defined above, there is an energy gap  $\hbar\pi/T$  between the quasienergies  $\lambda_0$  and  $\lambda_{2^n-1}$ . The corresponding Floquet states are given by  $|\Phi_0\rangle \approx (|0\rangle + |2^n - 1\rangle)/\sqrt{2}$  and  $|\Phi_{2^n-1}\rangle \approx (|0\rangle - |2^n - 1\rangle)/\sqrt{2}$ , which are maximally entangled GHZ states. The same behaviour is observed for other configurations,  $|i\rangle$  and  $|2^n - 1 - i\rangle$ , as all the paired Floquet states  $|\Phi_i\rangle$ ,  $|\Phi_{2^n-1-i}\rangle$  have an energy difference of  $\hbar\pi/T$  [9].

## VI. MELTING OF THE $2T$ -DTC

Consider now the case where our system is initialised to  $|\psi(0)\rangle = |2^n - 1\rangle = |\uparrow\uparrow\cdots\uparrow\rangle$  [10]. This state is a superposition of Floquet states,  $|\psi(0)\rangle \approx (|\Phi_0\rangle - |\Phi_{2^n-1}\rangle)/\sqrt{2}$  and in the graph is represented as a dimer between the nodes  $|0\rangle$  and  $|2^n - 1\rangle$ . Such a dimer remains decoupled and isolated for modest levels of error (up to a  $\sim 3\%$  error in the rotation added as a non-zero value of  $\epsilon$  in  $\hat{H}_1$ , see supplementary video). In Fig. 2 we present the effect of moderate ( $\epsilon = 0.012$ ) and large ( $\epsilon = 0.1$ ) levels of rotation errors  $\epsilon$  for a  $2T$ -DTC graph with  $n = 8$  spins. When the error increases there are couplings between the different subspaces and larger clusters appear in the graph (Fig. 2.a). If we keep increasing the error, the crystal will melt and its associated graph will take the form of a single highly –percolated– connected cluster (Fig. 2.d). The presence/no presence of such a dimer indicates whether the system is still in a crystalline phase or, otherwise, has been melted. This demonstrates how our graph strategy, among other things, can track the robustness of the system in a very visual and intuitive manner. Importantly, we note that not all dimers show the same robustness, and some of them survive to higher error values. This, in fact, allows us to identify the most convenient state initialization: the initial state corresponding to one of the configurations of the most robust dimer will make the crystal phase last longer.

## VII. CONSERVED QUANTITIES

Let us now analyze what factors are determinant in the robustness of each pair of configurations or, alternatively, how they cluster as the crystal melts. With our system represented as a graph, we can now focus on how to interpret its structural properties in terms of conserved quantities. To do so, it is of fundamental importance to note that the system is switching stroboscopically between two configurations,  $|i\rangle$  and  $|2^n - 1 - i\rangle$ . If we prepare the system in a symmetry broken state and observe the system every two periods ( $2T$ ), the system will effectively remain in a manifold of states with a fixed quasienergy. For no error, the graph will be formed by decoupled single nodes. In that sense, if we sample the dynamics every two

periods, the system is in an effective equilibrium state determined by conserved quantities that are defined stroboscopically. Now let us construct the conserved quantities in the absence of error and show how they are destroyed when clusters in the graph are formed (Fig. 3).

To calculate the conserved quantities, let us consider the square of the Floquet operator of Eq. (2), where  $\hat{H}_{\epsilon,2T}^{\text{eff}}$  is the effective Hamiltonian now over two periods ( $\hat{H}_{\epsilon,2T}^{\text{eff}} = i\hbar/2T \log[\hat{\mathcal{F}}_{\epsilon}^2]$ ). In that stroboscopic framework ( $2T$ ), the Floquet operator for no error can be reduced to the following expression:

$$\hat{\mathcal{F}}_{\epsilon=0}^2 = \exp\left(-2iT_2 \sum_{lm} J_{lm}^z \sigma_l^z \sigma_m^z\right). \quad (5)$$

In the absence of error,  $\epsilon = 0$ , the disorder cancels out exactly and the effective Hamiltonian reads  $\hat{H}_{\epsilon=0,2T}^{\text{eff}} = \hbar/2 \sum_{lm} J_{lm}^z \sigma_l^z \sigma_m^z$ . Despite its apparent simplicity, the effective Hamiltonian contains very relevant information. In particular, it preserves the total number of domain walls of the basis states  $\hat{N} = \sum_l (1 - \sigma_l^z \sigma_{l+1}^z)$  and parity  $\hat{\Pi} = \exp[i\pi/2 \sum_{l=1} (1 - \sigma_l^x + 1)]$  such that  $[\hat{H}_{\epsilon=0,2T}^{\text{eff}}, \hat{N}] = [\hat{H}_{\epsilon=0,2T}^{\text{eff}}, \hat{\Pi}] = 0$ . Therefore our conserved quantities are classified according to parity and the total number of domain walls. If we prepare the system in the initial state  $|\psi(0)\rangle = |2^n - 1\rangle$ , the system will remain stroboscopically within the symmetry multiplet with period-2 quasienergy  $\lambda_1^{2T} = \hbar/2 \sum_{lm} J_{lm}^z$  and zero domains walls  $\langle \hat{N} \rangle = 0$ . As shown in Fig. 1.c, in the absence of error, all the dimers conserve the number of domain walls (represented as a colormap) and their quasienergies. The aforementioned initial state, however, breaks the spatial parity symmetry  $\hat{\Pi}$ , which leads to a non-zero value of the correlation function  $\langle \sigma_l^z(\tau) \rangle = \langle \psi(0) | \sigma_l^z(\tau) \sigma_l^z(0) | \psi(0) \rangle \neq 0$ , as observed in the experiment [10].

## VIII. BREAKING SYMMETRIES

For zero error, the  $2^n$  quasienergies are local integrals of motion and the Hilbert space can be classified by using the symmetries that preserve the aforementioned conserved quantities. In turn, the effective Hamiltonian  $\hat{H}_{\epsilon,2T}^{\text{eff}}$  is block diagonal (see Fig. 3.b) with  $n$  sub-blocks given by the conservation of the number of domain walls. In the absence of error ( $\epsilon = 0$ ), and after  $2T$ , one can find a classical quasienergy surface in phase space associated to the effective Hamiltonian  $\hat{H}_{\epsilon=0,2T}^{\text{eff}}$ . The idea is to represent the spins as vectors in a three-dimensional space. By using polar coordinates, one can derive the classical Hamiltonian in a  $n$ -dimensional phase space

$$\mathcal{H}_{\epsilon=0,2T}^{\text{eff}}(\theta_1, \theta_2, \dots, \theta_n) = \frac{1}{2} \sum_{lm} J_{lm}^z \cos \theta_l \cos \theta_m, \quad (6)$$

where  $\theta_l$  is the polar angle. From this one can show that spin configurations with zero domain walls such as  $\theta_1 = \theta_2 = \dots = \theta_n$  are stable fixed points. Contrary to this, if a spin configuration has non-zero number of domain walls, it is an unstable

fixed point. If we consider the effect of the error, the system is far from the classical limit and quantum effects are dominant. To investigate this, we use the Baker-Campbell-Hausdorff formula to obtain, up to a first order approximation, the effective Hamiltonian for a non-zero value of  $\epsilon$ :

$$\hat{H}_{\epsilon,2T}^{\text{eff}} = \frac{\hbar}{2} \sum_{lm} J_{lm}^z \sigma_l^z \sigma_m^z - \frac{\hbar g \epsilon}{4} \sum_l [(\cos(B_l T) + 1) \sigma_l^x + \sin(B_l T) \sigma_l^y]. \quad (7)$$

This allows us to understand how  $\epsilon$  destroys the symmetries by coupling different symmetry multiplets. This can be observed from Fig. 3.b-e, as off-diagonal entries start populating the effective Hamiltonian matrix due to the error. This situation resembles the Kolmogorov-Arnold-Moser (KAM) theory in classical mechanics, which describes how invariant tori are broken in phase space under the effect of perturbations [28], with our perturbation being  $\epsilon$ . First of all, the transverse field term  $-\hbar g \epsilon / 4 \sum_l \sin(B_l T) \sigma_l^y$  breaks the parity symmetry. Most importantly, the transverse field term  $-\hbar g \epsilon / 4 \sum_l (\cos(B_l T) + 1) \sigma_l^x$ , while preserving parity, melts the ferromagnetic order and breaks the conservation of the number of domain walls. One of the most interesting aspects of our work is the striking similarity with KAM theory in classical systems: a small perturbation can destroy integrals of motion [28]. The most fragile integrals of motion are periodic unstable orbits in phase space as discussed in the context of Eq. (6). This explains the robustness of the time crystal and how clusters form in the graph, as we increase the error. The time crystal is robust against small errors because the last integral of motion that is destroyed by the perturbation is the configuration with the lowest number of domain walls: this is,  $|\Psi(0)\rangle = |2^n - 1\rangle$  (see darkest blue dimer on the top-right corner of Fig. 2.a).

## IX. PREFERENTIAL ATTACHMENT

Let us now put the focus on the network topology for moderate levels of rotation error ( $\epsilon \sim 0.012$ ). In the previous section we have seen that the quantum terms that appear in Eq. (7) break the conservation of number of domain walls. The error lifts the degeneracies present in the spectrum and new transitions between close states appear. In terms of the graph, the nodes with the same or similar number of domain walls connect following a preferential attachment mechanism. As most nodes in the network have  $n/2$  or  $n/2 - 1$  ( $n$ : even) number of domain walls, and they have very close quasienergies, these nodes easily connect to each other with a small value of error. This leads to the appearance of the large degree hub nodes as well as the heavy tailed degree distributions shown in Fig. 2.c. The tail of these distributions can be fit to a power law distribution, which is the characteristic of scale-free networks. Following Clauset *et al.*'s recommendations [29], we further test the goodness of fit of the power law against the lognormal distribution for each of these distributions, and observe that the power law favours over the lognormal distribution.

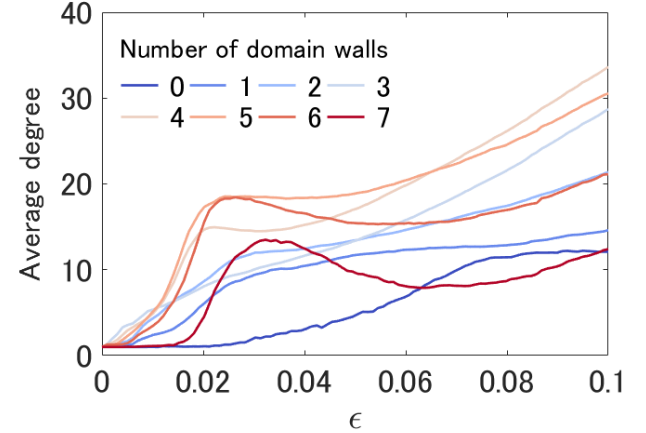


Figure 4. The average degree of the graph obtained from  $\hat{H}_{\epsilon,T}^{\text{eff}}$  with  $n = 8$  sites, plotted against the error  $\epsilon$ . The nodes are distinguished by their number of domain walls, and averaged individually for each values of domain walls, as well as averaging over 100 realizations of disorder. Notice that some of the curves exhibit a local maximum approximately between  $0.01 < \epsilon < 0.03$ . This is exactly the range in which we observe the scale-free behavior emerging in our system. Comparing each curves also confirms that the states with lower number of domain walls are more robust against the error in a sense that they have lower degrees.

In addition, exploring the behaviour of the average degree of the graph obtained from  $\hat{H}_{\epsilon,T}^{\text{eff}}$  further captures the existence of the preferential attachment mechanism and the non-trivial melting process of the 2T-DTC. From Fig. 4, we can confirm that the nodes with 5 or 6 domain walls (where the  $n = 8$  case is considered here) tend to acquire neighbours preferentially and have more degree already from a small error  $\epsilon < 0.02$ . This is the region where we can observe the scale-free behaviour emerging. When the error is increased, the preferential behaviour becomes weaker, and eventually most of the nodes tend to have large degree, closer to the structure of random networks, which indicates the crystal has melted.

This behaviour not only has consequences for the dynamics of the time crystals but can also be used to perform quantum simulation of networks with exotic properties such as scale-free-like ones [16]. Note that the scale-free-like networks shown in Fig. 2 are only observed in the effective Hamiltonian obtained from single period  $\hat{H}_{\epsilon,T}^{\text{eff}}$  and not in the one from two periods  $\hat{H}_{\epsilon,2T}^{\text{eff}}$ , which shows Poisson distributions, typical for random networks [16, 30]. We can understand this from the fact that the error induces local operations in the effective Hamiltonian  $\hat{H}_{\epsilon,2T}^{\text{eff}}$  up to a first-order approximation as shown in Eq. (7), which limits the number of allowed transitions. On the other hand, the off-diagonal terms of  $\hat{H}_{\epsilon,T}^{\text{eff}}$  contains non-local terms, which allows some states to have transitions to a large fraction of states in the Hilbert space. This indicates that non-local terms are necessary in order to simulate such scale-free-like networks.

## X. CONCLUSIONS

Our approach of representing discrete time crystals in terms of graphs is key to understand the structure of such an exotic phase of matter and to envisage prospective applications. We explicitly show that by translating a  $2T$ -DTC into a graph theory language we can study in detail how the crystal order disappears as an increasing error melts the time crystal. Among others, it allowed us to identify the crucial role symmetries and conserved quantities play in the resilience of the crystal, by observing the preferential attachment mechanism present in the formation of clusters. Crucially, the nature of the obtained graphs for moderate levels of error suggests that such systems could be used as scale-free-like network simulators, giving rise to a novel application of such devices in the field of complex networks. Importantly, because our networks span the configuration space, such simulation could be done with moderate numbers of qubits and thus available noisy intermediate-scale quantum (NISQ) platforms (ranging from ion traps to superconducting qubit chips) could be used for its implementation. Future work will include further inves-

tigation and characterization on the nature of these networks as well as the study of additional phenomena present in time crystals in terms of graphs. We believe that the use of this formalism will lead not only to a more complete and deep understanding of discrete time crystals and their related phenomena, but also be very advantageous in the study of periodically driven quantum systems.

*Acknowledgement:*— We thank M. Hanks, T. Haug, Y. Naka Renoust, and J. Schmiedmayer for valuable discussions. This work was supported in part from the Japanese program Q-LEAP, the MEXT KAKENHI Grant-in-Aid for Scientific Research on Innovative Areas Science of hybrid quantum systems Grant No.15H05870 and the JSPS KAKENHI Grant No. 19H00662. This project was also made possible through the support of a grant from the John Templeton Foundation (JTF 60478). The opinions expressed in this publication are those of the authors and do not necessarily reflect the views of the John Templeton Foundation.

---

[1] S. L. Sondhi, S. M. Girvin, J. P. Carini, and D. Shahar, *Rev. Mod. Phys.* **69**, 315 (1997).

[2] P. W. Higgs, *Phys. Rev. Lett.* **13**, 508 (1964).

[3] J. Bardeen, L. N. Cooper, and J. R. Schrieffer, *Phys. Rev.* **108**, 1175 (1957).

[4] G. M. Luke, Y. Fudamoto, K. M. Kojima, M. I. Larkin, J. Merrin, B. Nachumi, Y. J. Uemura, Y. Maeno, Z. Q. Mao, Y. Mori, H. Nakamura, and M. Sigrist, *Nature* **394**, 558 (1998).

[5] K. Sacha and J. Zakrzewski, *Reports on Progress in Physics* **81**, 016401 (2018).

[6] F. Wilczek, *Phys. Rev. Lett.* **109**, 160401 (2012).

[7] K. Sacha, *Phys. Rev. A* **91**, 033617 (2015).

[8] D. V. Else, B. Bauer, and C. Nayak, *Phys. Rev. Lett.* **117**, 090402 (2016).

[9] V. Khemani, A. Lazarides, R. Moessner, and S. L. Sondhi, *Phys. Rev. Lett.* **116**, 250401 (2016).

[10] J. Zhang, P. W. Hess, A. Kyprianidis, P. Becker, A. Lee, J. Smith, G. Pagano, I.-D. Potirniche, A. C. Potter, A. Vishwanath, N. Y. Yao, and C. Monroe, *Nature* **543**, 217 (2017).

[11] S. Choi, J. Choi, R. Landig, G. Kucsko, H. Zhou, J. Isoya, F. Jelezko, S. Onoda, H. Sumiya, V. Khemani, C. von Keyserlingk, N. Y. Yao, E. Demler, and M. D. Lukin, *Nature* **543**, 221 (2017).

[12] J. Rovny, R. L. Blum, and S. E. Barrett, *Phys. Rev. Lett.* **120**, 180603 (2018).

[13] N. Y. Yao, A. C. Potter, I.-D. Potirniche, and A. Vishwanath, *Phys. Rev. Lett.* **118**, 030401 (2017).

[14] K. Giergiel, A. Kosior, P. Hannaford, and K. Sacha, *Phys. Rev. A* **98**, 013613 (2018).

[15] A.-L. Barabási and R. Albert, *Science* **286**, 509 (1999).

[16] R. Albert and A.-L. Barabási, *Rev. Mod. Phys.* **74**, 47 (2002).

[17] S. Yong, W. Xiangming, Z. Zhenmin, and L. Yuan, *2012 7th International Conference on Computer Science Education (ICCSE)*, , 390 (2012).

[18] C. Trabelsi, O. Bilaniuk, Y. Zhang, D. Serdyuk, S. Subramanian, J. F. Santos, S. Mehri, N. Rostamzadeh, Y. Bengio, and C. J. Pal, *International Conference on Learning Representations*, (2018).

[19] S. N. Dorogovtsev and J. F. F. Mendes, *Evolution of Networks: From Biological Nets to the Internet and WWW (Physics)* (Oxford University Press, Inc., New York, NY, USA, 2003).

[20] M. Grifoni and P. Hänggi, *Physics Reports* **304**, 229 (1998).

[21] M. Bukov, L. D’Alessio, and A. Polkovnikov, *Advances in Physics* **64**, 139 (2015).

[22] A. Eckardt and E. Anisimovas, *New Journal of Physics* **17**, 093039 (2015).

[23] S. Restrepo, J. Cerrillo, V. M. Bastidas, D. G. Angelakis, and T. Brandes, *Phys. Rev. Lett.* **117**, 250401 (2016).

[24] A. Eckardt, *Rev. Mod. Phys.* **89**, 011004 (2017).

[25] V. M. Bastidas, B. Renoust, K. Nemoto, and W. J. Munro, *Phys. Rev. B* **98**, 224307 (2018).

[26] S. Roy, J. T. Chalker, and D. E. Logan, *Phys. Rev. B* **99**, 104206 (2019).

[27] A. C. Potter, R. Vasseur, and S. A. Parameswaran, *Phys. Rev. X* **5**, 031033 (2015).

[28] V. F. Lazutkin, in *KAM Theory and Semiclassical Approximations to Eigenfunctions* (Springer Berlin Heidelberg, Berlin, Heidelberg, 1993) pp. 121–159.

[29] A. Clauset, C. Shalizi, and M. Newman, *SIAM Review* **51**, 661 (2009).

[30] M. Faccin, T. Johnson, J. Biamonte, S. Kais, and P. Migdał, *Phys. Rev. X* **3**, 041007 (2013).

## METHODS

### A. Floquet theory: Percolation rule and graph structure

One of the main tools used in our work is the percolation rule, which establishes when there is a link between two nodes of a graph representing the effective Hamiltonian. In this section we explain in detail the motivation of the percolation rule and its interpretation in terms of Floquet theory. In order to have an intuitive picture of the percolation rule, let us consider only two configurations  $|i\rangle$  and  $|j\rangle$  with energies  $E_i$  and  $E_j$  in the absence of drive, respectively. For simplicity, let us assume that the drive induces transitions only between the aforementioned configurations. Within the two-state approximation, the Hamiltonian from Eq.(1) reads:

$$\hat{H}(t) = \begin{cases} \hat{H}_1 \equiv \hbar g (1 - \epsilon) (|i\rangle\langle j| + |j\rangle\langle i|) & 0 < t < T_1 \\ \hat{H}_2 \equiv E_i |i\rangle\langle i| + E_j |j\rangle\langle j| & T_1 < t < T_2 \end{cases} \quad (8)$$

In general, the transitions occur when the driving is resonant with the energy level spacing between two configurations, i.e., when  $E_j - E_i = \hbar m \omega$ , where  $m$  is an integer and  $\omega = 2\pi/T$  is the frequency of the drive. Therefore, when the drive is switched on, the quasienergies  $\lambda_{s_1}$  and  $\lambda_{s_2}$  corresponding to the energies  $E_i$  and  $E_j$ , exhibit an anticrossing [20]. In the language of Floquet theory, the latter is referred to as a  $m$ -photon resonance because the quasienergies are defined modulo  $\omega$ .

If we restrict ourselves to the configurations  $|i\rangle$  and  $|j\rangle$ , the effective Hamiltonian can be written as

$$\hat{H}_{\epsilon,T}^{\text{eff}} = \mathcal{E}_i |i\rangle\langle i| + \mathcal{E}_j |j\rangle\langle j| + K_{ij} |i\rangle\langle j| + K_{ji} |j\rangle\langle i| = \lambda_{s_1} |\Phi_{s_1}\rangle\langle\Phi_{s_1}| + \lambda_{s_2} |\Phi_{s_2}\rangle\langle\Phi_{s_2}|. \quad (9)$$

From this we can see that the energy gap for the quasienergies scales as  $\delta\lambda = |\lambda_{s_1} - \lambda_{s_2}| = \sqrt{(\mathcal{E}_i - \mathcal{E}_j)^2 + (K_{ij})^2}$ . In addition, we can derive the expressions for the eigenstates  $|\Phi_{s_1}\rangle = \cos\theta_{ij}|i\rangle + \sin\theta_{ij}|j\rangle$  and  $|\Phi_{s_2}\rangle = -\sin\theta_{ij}|i\rangle + \cos\theta_{ij}|j\rangle$ , where  $\cos\theta_{ij} = |\mathcal{E}_i - \mathcal{E}_j|/\delta\lambda$  and  $\sin\theta_{ij} = |K_{ij}|/\delta\lambda$ . The percolation rule  $|\mathcal{E}_j - \mathcal{E}_i| < |K_{ij}|$  from Eq. (4) implies that when the link between the  $i$ -th and  $j$ -th nodes is active, the Floquet states  $|\Phi_{s_1}\rangle$  and  $|\Phi_{s_2}\rangle$  with quasienergies  $\lambda_{s_1}$  and  $\lambda_{s_2}$  are delocalized in the basis  $|i\rangle$  and  $|j\rangle$ . On the contrary, if the percolation rule is violated, i.e.,  $|\mathcal{E}_j - \mathcal{E}_i| > |K_{ij}|$ , the Floquet states are localized and no link between the  $i$ -th and  $j$ -th nodes is drawn in the graph.

### B. Power law fitting of the degree distributions

Here we explain how the degree distributions of the graphs obtained from the effective Hamiltonian of the  $2T$ -DTC can be fit to a power law function  $p(k) \propto k^{-\beta}$ . We have followed the method by Clauset *et al.* [29]. First, the degree distributions  $P(k)$  are obtained by measuring log-binned histograms of the degrees  $k$  of the graph. We have obtained the distributions from 100 realizations of the graph with different disorder values for statistical convergence. Generally, the power law behaviour is observed in the large degree tail of the distribution rather than the entire domain. Therefore, we estimate the lower bound  $k = k_{\min}$  where the best power law fit can be obtained. This is done by estimating the power law exponent  $\beta$  by applying maximum likelihood method on a certain portion  $k \geq k_{\text{cutoff}}$  of the distribution. Once the exponent is estimated, the Kolmogorov-Smirnov distance between the distribution and the fit is computed. We compute this with various  $k_{\text{cutoff}} > 0$  and the  $k_{\min}$  is chosen at the  $k_{\text{cutoff}}$  where the Kolmogorov-Smirnov distance is minimized. Once the  $k_{\min}$  and  $\beta$  is estimated, we examine the goodness of fit of the power law using a comparative test. We consider an alternative probability distribution function that may be good fit for our data, and apply a likelihood ratio test between the power law and the alternative function. Here we chose the lognormal function as the alternative, which is another heavy-tailed function. From this comparative test, we conclude that the power law function well describes the degree distributions of our graphs.